Deducing Ground-to-Air Emissions from Observed Trace Gas Concentrations: A Field Trial with Wind Disturbance

T. K. FLESCH AND J. D. WILSON

Department of Earth and Atmospheric Sciences, University of Alberta, Edmonton, Alberta, Canada

L. A. HARPER

Agricultural Research Service, USDA, Watkinsville, Georgia

(Manuscript received 26 April 2004, in final form 30 September 2004)

ABSTRACT

Inverse-dispersion techniques allow inference of a gas emission rate Q from measured air concentration. In "ideal surface layer problems," where Monin–Obukhov similarity theory (MOST) describes the winds transporting the gas, the application of the technique can be straightforward. This study examines the accuracy of an ideal MOST-based inference, but in a nonideal setting. From a 6 m × 6 m synthetic area source surrounded by a 20 m × 20 m square border of a windbreak fence (1.25 m tall), Q is estimated. Open-path lasers gave line-averaged concentration C_L at positions downwind of the source, and an idealized backward Lagrangian stochastic (bLS) dispersion model was used to infer Q_{bLS}. Despite the disturbance of the mean wind and turbulence caused by the fence, the Q_{bLS} estimates were accurate when ambient winds (measured upwind of the plot) were assumed in the bLS model. In the worst cases, with C_L measured adjacent to a plot fence, Q_{bLS} overestimated Q by an average of 50%. However, if these near-fence locations are eliminated, Q_{bLS} averaged within 2% of the true Q over 61 fifteen-minute observations (with a standard deviation $\sigma_{\mathrm{Q/Q}} = 0.20$). Poorer accuracy occurred when in-plot wind measurements were used in the bLS model. The results show that when an inverse-dispersion technique is applied to disturbed flows without accounting for the disturbance, the outcome may still be of acceptable accuracy if judgment is applied in the placement of the concentration detector.

1. Introduction

Inverse-dispersion calculations provide an attractive technique for inferring ground-to-air emissions. Consider an area source emitting tracer at a uniform but unknown rate Q (kg m^{-2} s^{-1}), with a measurement of line-averaged tracer concentration C_L (g m^{-3}) taken in the resultant plume (Fig. 1a). Given a theoretical ratio $(C_L/Q)_{\mathrm{sim}}$, provided by an atmospheric dispersion model, one may assume

$$Q = (C_L - C_b)/(C_L/Q)_{\mathrm{sim}}, \tag{1}$$

where C_b is the background tracer concentration. This approach has several potential advantages over other measurement techniques—simple field observations, no fundamental restrictions on the size or shape of the source, and flexibility in the location of the concentration measurement.

In a recent companion paper (Flesch et al. 2004) we describe how a modern Lagrangian (particle tracking) dispersion model can be applied to calculate $(C_L/Q)_{\mathrm{sim}}$ in "ideal surface layer problems." These are situations in which Monin–Obukhov similarity theory (MOST) describes the winds near the ground (see Garratt 1992), with wind statistics determined from the friction velocity u_*, the Obukhov stability length L, the average wind direction β, and the surface roughness length z_0—properties that can be measured from the surface with reasonable ease. If the source and concentration sensor lie within a homogeneous landscape, and the source-to-sensor distance is sufficiently short so that tracer paths remain in the surface layer, application of the inverse-dispersion technique can be straightforward.[1]

Unfortunately, the real world seldom provides truly ideal surface layer problems. Consider a hypothetical livestock feedlot as an emission source (Fig. 1b). From afar its geometry is similar to the ideal in Fig. 1a, but

Corresponding author address: T. K. Flesch, Department of Earth and Atmospheric Sciences, University of Alberta, Edmonton, AB T6G 2E3, Canada.
E-mail: thomas.flesch@ualberta.ca

[1] The works of Wilson et al. (1982), McInnes et al. (1985), and Lehning et al. (1994) are examples in which idealized dispersion models are used to infer emissions.

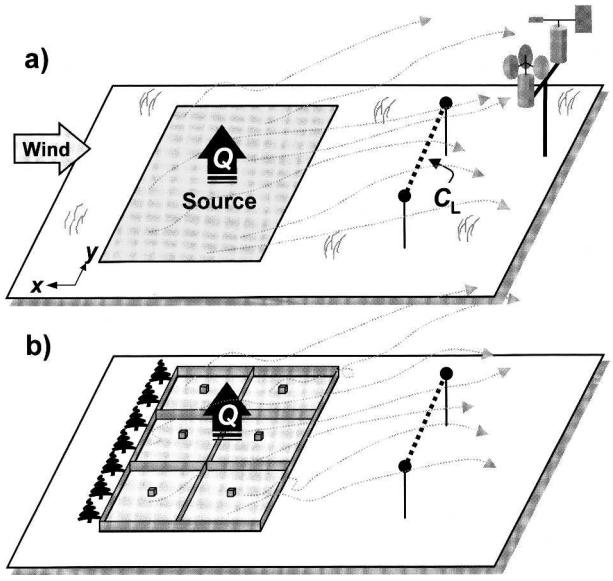

FIG. 1. Application of the inverse-dispersion technique for calculating emission rate Q. Line-averaged concentration (C_L) is measured downwind of a source, and $(C_L/Q)_{\text{sim}}$ is calculated with a dispersion model; (a) a problem with no wind complexity, and (b) an example in which obstacles (fence, trees, etc.) cause wind complexity.

upon focusing on the detail we see an environment that is characterized by wind disturbances. Fences, shelterbelts, animals, and buildings introduce vortices, jets, and sheltered zones. A change in surface characteristics over the feedlot (e.g., roughness, moisture) will act to create a new wind regime that is different from that over the surrounding landscape. The result is a unique wind environment where MOST does not apply. How can one use the inverse-dispersion technique here? The rigorous approach would be to incorporate the correct (disturbed) wind field in calculating $(C_L/Q)_{\text{sim}}$. Yet comprehensive *measurement* of the wind field is generally beyond practical capabilities, and *modeling* of the wind (e.g., using Reynolds-averaged Navier–Stokes equations) is a complex task and results in wind predictions that may not be very accurate (e.g., Wilson and Yee 2003).

Another option is to use idealized dispersion models and ignore the wind complexity. For example, Wilson et al. (2001) simulated the disturbed winds around a lagoon that was aerodynamically smoother and either warmer (night) or colder (day) than the surrounding ground. This resulted in the development of an internal boundary layer over the lagoon. Despite the wind complexity, the emissions diagnosed from a MOST-based dispersion model, using observations of concentration and wind over the lagoon, were calculated to be within 15% of the true Q, except in the most extreme case. This compromised, yet still useful, level of accuracy can justify the preference for a simple MOST-based calculation.

Here we describe a field experiment in which the inverse-dispersion technique was used to infer emissions in a setting analogous to Fig. 1b. We surrounded a surface source of known Q with a border of windbreak fence that perturbs the wind. Concentration C_L was measured downwind of the source, and a MOST-based backward Lagrangian stochastic (bLS) dispersion model was used to infer the emission rate Q_{bLS}. Our objectives were to 1) quantify the accuracy in Q_{bLS} in a disturbed wind setting, 2) find to what extent measurement location affects the accuracy of our inference in disturbed flows, and 3) generalize how one should employ a simple MOST-based approach to infer emissions in the real world.

2. Field experiment

This study is a reconfiguration of the experiment of Flesch et al. (2004) and we direct the reader to this companion paper for a complete description of the experimental details and the bLS dispersion model. Here we summarize this material and expand on the new features of this study.

a. Emission source

Methane (CH_4) was released from a small surface source during 4 days in May and June 2001, near Ellerslie, Alberta, Canada. The release site was an alfalfa–clover field, covered in stubble and low vegetation (height of 0.05–0.10 m). From a meteorological perspective the site was ideal, with uniform land extending upwind a minimum of 500 m from the release site. Our source was a manifold with 36 outlets on a square grid, constructed to approximate a 6 m $\times$ 6 m surface area source (see Fig. 2). A high pressure methane cylinder was coupled to the manifold through a regulator and flowmeter. A porous windbreak fence (with height h = 1.25 m, resistance coefficient k_{ro} = 2.4, porosity ρ = 0.45) surrounded the source, forming a 20 m $\times$ 20 m square border with the source in the middle. The fence dramatically disturbs the ambient winds. Gas releases took place in near-neutral stratification. Dates, times, and meteorological conditions during the releases are given in Table 1.

b. Concentration measurements

The line-averaged methane concentration C_L was measured with two open-path lasers (GasFinders, Boreal Laser, Inc., Edmonton, Alberta, Canada[2]), and averaged into 15-min values. To convert the reported mixing-ratio concentrations (ppm) to absolute concen-

[2] Listing of source names is for the information of the reader and does not imply endorsement or preferential treatment by the University of Alberta or the U.S. Department of Agriculture.

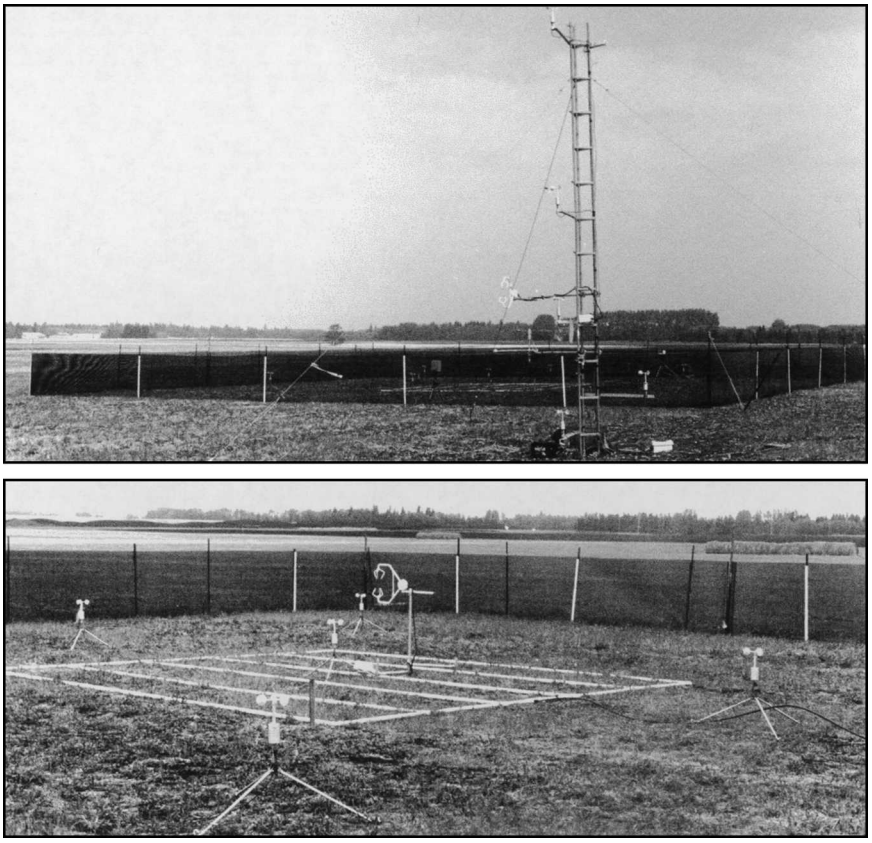

FIG. 2. The experimental site: (top) the fenced plot and the upwind tower where ambient winds are measured, and (bottom) the tracer source at the center of the fenced plot (the cup anemometers were not used in this study).

tration (g m^{-3}) we used the air temperature for each observation period and assumed an air pressure of 930 hPa, the average surface pressure for the area. Background concentration C_b was measured from each laser for 5–15 min before and after gas release (waiting 5 min after the release ended to allow for a return to the background). There was no C_b measurement during the release, and we assumed that C_b trended linearly with time between the "before" and "after" measurements.

During the experiment the lasers were placed in eight different positions around the source (Fig. 3), with pathlengths ranging from 18 to 196 m. Lasers and retroreflectors were positioned 1.0 m above the ground. We took the average of the path-center height and the laser/reflector height as the measurement height z_m in the bLS simulations. Five release periods (10 h of gas release) and two lasers gave a total of 10 experimental trials.

c. Meteorological observations

Two three-dimensional sonic anemometers (CSAT-3, Campbell Scientific, Inc., Logan, Utah) were used to measure winds. The first anemometer was placed on an upwind tower at height $z_{son} \sim 2$ m above ground (the height varied slightly during the experiment), and this gave the ambient wind conditions (i.e., u_*, z_0, L, β). The second was placed in the center of the fenced plot ($z_{son} \sim 1$ m). These anemometers were repositioned as necessary to ensure a frontal approach flow and to avoid the tower wake. Wind velocity and acoustic temperature were sampled at a frequency of 16 Hz.

Raw velocity and heat flux statistics were transformed using a double rotation (Kaimal and Finnigan 1994). No spectral corrections were made to the sonic anemometer signals.[3] From these statistics we calculated the friction velocity u_*, the Obukhov length L, and the roughness length z_0 as described in Flesch et al. (2004).

3. Fence effects on the wind

The wind environment within our fenced plot is very different from the undisturbed approach winds (see

[3] We calculate that the errors in heat and momentum fluxes caused by frequency attenuation will be less than 5% (following Massman 2000, or Horst 1997), assuming ideal flat-terrain turbulent spectra. The error in the in-plot sonic anemometer may be higher if the spectra are shifted toward higher frequencies (although we believe it will still be relatively small).

TABLE 1. Gas release observations. Laser and reflector positions for each trial are referenced to the (x, y) corners of the 6 m × 6 m source at (−0.5, 0.5), (5.5, 0.7), (−0.3, −5.5), and (5.7, −5.3), where x and y are the east–west and north–south coordinates (m), respectively. The average along-wind velocity (U), friction velocity u_*, Obukhov length L, roughness length z_0, and average wind direction β are given from both the upwind and in-plot anemometers (the subscript "p" indicates in-plot estimates). Measured concentration C_L, assumed background concentration C_b, and the actual emission rate Q are also given.

Time (LST)	U (m s^{-1})	β (°)	u_* (m s^{-1})	L (m)	z_0 (m)	U_p (m s^{-1})	β_p (°)	u_{*p} (m s^{-1})	L_p (m)	$z_{0\text{-}p}$ (m)	Q (g m^{-2} s^{-1})	C_L (ppm)	C_b (ppm)
F2–5; day 148; ambient/in-plot z_{son}: 2.2/0.97 m; avg T = 25°C; laser/reflector positions (x, y, z_m): −6.3, 0.1, 1.0/12.0, −0.5, 1.0													
1315	12.85	133	0.88	−198	0.0061	10.33	134	0.85	−346	0.0073	0.0135	3.06	1.94
1330	13.17	132	0.88	−197	0.0053	10.50	134	0.86	−281	0.0073	0.0135	2.97	1.91
1345	12.88	137	0.88	−196	0.0061	9.72	136	0.94	−436	0.0153	0.0135	3.12	1.87
1500	12.45	133	0.85	−207	0.0060	9.00	135	0.90	−451	0.0178	0.0135	3.06	1.70
F2–6; day 148; ambient/in-plot z_{son}: 2.2/0.97 m; avg T = 25°C; laser/reflector positions (x, y, z_m): −32, 9.5, 1.0/20.3, 8.7, 1.0													
1315	12.85	133	0.88	−198	0.0061	10.33	134	0.85	−346	0.0073	0.0135	3.42	1.79
1330	13.17	132	0.88	−197	0.0053	10.50	134	0.86	−281	0.0073	0.0135	3.38	1.80
1430	13.70	134	0.93	−221	0.0059	10.71	135	0.92	−444	0.0093	0.0135	3.36	1.82
1500	12.45	133	0.85	−207	0.0060	9.00	135	0.90	−451	0.0178	0.0135	3.38	1.83
F3–5; day 151; ambient/in-plot z_{son}: 2.2/0.97 m; avg T = 15°C; laser/reflector positions (x, y, z_m): 6.7, 5.9, 0.95/5.5, −12.7, 0.95													
1015	5.57	337	0.41	−43	0.0082	3.20	325	0.59	−146	0.1093	0.0135	8.94	2.09
1030	5.62	337	0.46	−54	0.0145	3.06	325	0.65	−146	0.1423	0.0135	9.26	2.09
1045	5.57	338	0.46	−53	0.0150	3.02	327	0.61	−131	0.1319	0.0135	9.70	2.10
1130	7.08	329	0.53	−69	0.0094	4.99	320	0.69	−205	0.0518	0.0135	5.69	2.11
1145	5.98	323	0.47	−49	0.0116	3.84	318	0.55	−109	0.0586	0.0135	6.99	2.11
1200	5.41	316	0.42	−33	0.0104	3.79	314	0.48	−71	0.0396	0.0135	6.93	2.11
1215	6.21	307	0.47	−37	0.0093	4.29	309	0.58	−114	0.0495	0.0135	6.20	2.11
F3–6; day 151; ambient/in-plot z_{son}: 2.2/0.97 m; avg T = 15°C; laser/reflector positions (x, y, z_m): −21.5, −134.3, 0.85/96.5, 21.8, 0.85													
1015	5.57	337	0.41	−43	0.0082	3.20	325	0.59	−146	0.1093	0.0135	1.94	1.82
1030	5.62	337	0.46	−54	0.0145	3.06	325	0.65	−146	0.1423	0.0135	1.94	1.81
1045	5.57	338	0.46	−53	0.0150	3.02	327	0.61	−131	0.1319	0.0135	1.93	1.80
1130	7.08	329	0.53	−69	0.0094	4.99	320	0.69	−205	0.0518	0.0135	1.92	1.80
1145	5.98	323	0.47	−49	0.0116	3.84	318	0.55	−109	0.0586	0.0135	1.95	1.82
1200	5.41	316	0.42	−33	0.0104	3.79	314	0.48	−71	0.0396	0.0135	2.03	1.84
1215	6.21	307	0.47	−37	0.0093	4.29	309	0.58	−114	0.0495	0.0135	2.01	1.87
F4–5; day 151; ambient/in-plot z_{son}: 2.2/0.97 m; avg T = 12°C; laser/reflector positions (x, y, z_m): 6.7, 5.9, 0.95/5.5, −12.7, 0.95													
1415	6.11	342	0.50	−40	0.0138	2.88	330	0.66	−112	0.1642	0.0090	5.84	1.96
1430	5.61	335	0.45	−32	0.0121	2.98	325	0.64	−90	0.1445	0.0090	5.98	1.97
1445	6.63	349	0.55	−59	0.0155	2.54	339	0.73	−119	0.2345	0.0135	7.58	1.97
1500	6.02	340	0.50	−44	0.0151	2.81	330	0.67	−114	0.1763	0.0135	8.88	1.98
1515	5.70	340	0.42	−31	0.0078	2.74	328	0.64	−101	0.1702	0.0135	9.13	1.98
1530	5.51	338	0.44	−32	0.0119	3.09	326	0.57	−85	0.1048	0.0135	8.65	1.98
1545	5.11	355	0.32	−17	0.0026	1.93	350	0.55	−64	0.2286	0.0090	5.07	1.98
1600	5.19	336	0.35	−20	0.0043	3.05	325	0.56	−99	0.1065	0.0090	6.64	1.99
1615	5.58	347	0.40	−32	0.0067	2.32	337	0.64	−123	0.2202	0.0090	6.34	1.99
F4–6; day 151; ambient/in-plot z_{son}: 2.2/0.97 m; avg T = 12°C; laser/reflector positions (x, y, z_m): −16.5, −53.5, 0.95/57.8, 8.9, 0.95													
1415	6.11	342	0.50	−40	0.0138	2.88	330	0.66	−112	0.1642	0.0090	2.06	1.77
1430	5.61	335	0.45	−32	0.0121	2.98	325	0.64	−90	0.1445	0.0090	2.19	1.79
1445	6.63	349	0.55	−59	0.0155	2.54	339	0.73	−119	0.2345	0.0135	2.22	1.80
1500	6.02	340	0.50	−44	0.0151	2.81	330	0.67	−114	0.1763	0.0135	2.31	1.80
1515	5.70	340	0.42	−31	0.0078	2.74	328	0.64	−101	0.1702	0.0135	2.31	1.82
1530	5.51	338	0.44	−32	0.0119	3.09	326	0.57	−85	0.1048	0.0135	2.33	1.82
1545	5.11	355	0.32	−17	0.0026	1.93	350	0.55	−64	0.2286	0.0090	2.10	1.83
1600	5.19	336	0.35	−20	0.0043	3.05	325	0.56	−99	0.1065	0.0090	2.21	1.84
1615	5.58	347	0.40	−32	0.0067	2.32	337	0.64	−123	0.2202	0.0090	2.18	1.85
F5–5; day 152; ambient/in-plot z_{son}: 2.2/0.97 m; avg T = 20°C; laser/reflector positions (x, y, z_m): −6.3, 0.1, 1.0/12.0, −0.5, 1.0													
1445	8.84	131	0.69	−93	0.0120	6.57	137	0.65	−177	0.0165	0.0135	3.97	1.73
1500	8.95	129	0.65	−85	0.0082	5.86	135	0.76	−176	0.0431	0.0135	4.76	1.76
1515	9.27	134	0.69	−117	0.0095	6.97	138	0.68	−242	0.0159	0.0135	3.95	1.79
1530	8.88	136	0.62	−128	0.0067	6.42	138	0.73	−319	0.0283	0.0135	4.12	1.83
1600	8.70	133	0.64	−190	0.0092	6.62	137	0.71	−474	0.0229	0.0090	3.22	1.85
1615	8.77	139	0.66	−206	0.0104	7.14	140	0.63	−488	0.01	0.0090	3.11	1.86
1630	9.24	141	0.69	−235	0.0100	6.89	141	0.72	−518	0.0205	0.0090	3.39	1.86
1645	9.60	139	0.73	−232	0.0110	8.09	140	0.65	−346	0.0068	0.0090	2.90	1.87

TABLE 1. (*Continued*)

Time (LST)	U (m s^{-1})	β (°)	u_* (m s^{-1})	L (m)	z_0 (m)	U_p (m s^{-1})	β_p (°)	u_{*p} (m s^{-1})	L_p (m)	$z_{0\text{-}p}$ (m)	Q (g m^{-2} s^{-1})	C_L (ppm)	C_b (ppm)
F5–6; day 152; ambient/in-plot z_{son}: 2.2/0.97 m; avg T = 20°C; laser/reflector positions (x, y, z_m): −19.9, −10.7, 1.0/6.0, 79.0, 1.0													
1445	8.84	131	0.69	−93	0.0120	6.57	137	0.65	−177	0.0165	0.0135	2.47	1.86
1500	8.95	129	0.65	−85	0.0082	5.86	135	0.76	−176	0.0431	0.0135	2.43	1.87
1515	9.27	134	0.69	−117	0.0095	6.97	138	0.68	−242	0.0159	0.0135	2.51	1.87
1530	8.88	136	0.62	−128	0.0067	6.42	138	0.73	−319	0.0283	0.0135	2.52	1.88
1600	8.70	133	0.64	−190	0.0092	6.62	137	0.71	−474	0.0229	0.0090	2.30	1.88
1615	8.77	139	0.66	−206	0.0104	7.14	140	0.63	−488	0.01	0.0090	2.34	1.89
1630	9.24	141	0.69	−235	0.0100	6.89	141	0.72	−518	0.0205	0.0090	2.31	1.89
1645	9.60	139	0.73	−232	0.0110	8.09	140	0.65	−346	0.0068	0.0090	2.31	1.90
F6–5; day 156; ambient/in-plot z_{son}: 2.2/0.98 m; avg T = 15°C; laser/reflector positions (x, y, z_m): −1.3, 6.3, 1.0/−2.4, −12.6, 1.0													
1045	4.26	140	0.35	−30	0.0135	3.02	139	0.33	−43	0.0239	0.0090	6.30	1.85
1100	4.65	120	0.36	−29	0.0100	2.67	130	0.43	−58	0.0791	0.0090	6.73	1.87
1115	4.82	135	0.37	−35	0.0098	3.69	138	0.38	−56	0.0178	0.0090	5.09	1.88
1130	4.14	150	0.33	−35	0.0120	2.68	145	0.39	−82	0.0596	0.0090	6.99	1.89
1145	5.34	145	0.44	−43	0.0144	3.65	143	0.51	−89	0.0545	0.0090	6.11	1.90
1200	5.86	150	0.49	−52	0.0159	3.76	144	0.59	−108	0.0739	0.0090	6.26	1.92
1215	5.94	136	0.45	−134	0.0105	4.56	137	0.46	−240	0.0179	0.0090	4.41	1.93
F6–6; day 156; ambient/in-plot z_{son}: 2.2/0.98 m; avg T = 15°C; laser/reflector positions (x, y, z_m): −46.2, 112.5, 1.0/−51.7, −26.0, 1.0													
1045	4.26	140	0.35	−30	0.0135	3.02	139	0.33	−43	0.0239	0.0090	1.92	1.78
1100	4.65	120	0.36	−29	0.0100	2.67	130	0.43	−58	0.0791	0.0090	1.93	1.78
1115	4.82	135	0.37	−35	0.0098	3.69	138	0.38	−56	0.0178	0.0090	1.96	1.79
1130	4.14	150	0.33	−35	0.0120	2.68	145	0.39	−82	0.0596	0.0090	1.91	1.79
1145	5.34	145	0.44	−43	0.0144	3.65	143	0.51	−89	0.0545	0.0090	1.93	1.80
1200	5.86	150	0.49	−52	0.0159	3.76	144	0.59	−108	0.0739	0.0090	1.95	1.80
1215	5.94	136	0.45	−134	0.0105	4.56	137	0.46	−240	0.0179	0.0090	1.96	1.80
1230	5.46	134	0.42	−103	0.0112	3.71	136	0.51	−328	0.0531	0.0090	1.94	1.80
1345	5.87	125	0.41	−84	0.0066	3.68	132	0.53	−307	0.0614	0.0090	2.12	1.96
1400	5.41	135	0.42	−100	0.0118	4.19	136	0.43	−175	0.0193	0.0090	2.16	1.96
1415	6.22	135	0.48	−118	0.0116	4.85	138	0.50	−204	0.0197	0.0090	2.14	1.96
1430	6.66	135	0.47	−151	0.0072	5.18	138	0.50	−357	0.0155	0.0090	2.13	1.96
1445	6.41	129	0.45	−80	0.0067	4.33	135	0.56	−211	0.0437	0.0090	2.12	1.96
1500	6.60	128	0.48	−141	0.0085	4.44	134	0.57	−369	0.0418	0.0090	2.13	1.96
1515	6.13	130	0.48	−156	0.0127	4.49	135	0.47	−315	0.0219	0.0090	2.14	1.96
1530	6.26	128	0.45	−84	0.0077	4.12	134	0.53	−181	0.044	0.0090	2.14	1.96

Fig. 4). Here, we reiterate the findings of Wilson and Flesch (2003), who made detailed wind observations at the site. As expected, the fence creates shelter inside the plot (i.e., there is an average wind speed reduction), but the degree of shelter is very sensitive to the angle of the approach wind. We use Wilson and Flesch's definition of reduced wind direction β_r, where by symmetry the orientation of all ambient wind directions can be represented as lying between $\beta_r = 0$ (perpendicular to a fence face, "normal flow") and 45° (oriented along a plot diagonal, "corner flow"). Now consider the average wind speed S at one-half times the fence height, $z/h = 0.5$ (Fig. 5). For normal flow S is below 50% of the ambient wind over about one-half of the plot. Yet for corner flow only about one-fifth of the plot sees S below 50%, with a high-speed jet along the plot diagonal. For intermediate β_r the pattern falls between these extremes. We surmise that the S immediately upwind and downwind of the plot is reduced from the ambient wind, with a speedup along the sides of the plot.

Strong horizontal gradients in S inside the plot indicate updrafts and downdrafts. We anticipate that during normal flow there will be weak updrafts along the upwind quarter of the plot (for height $z < h$), with the downwind portion of the plot experiencing downdrafts. Beside the downwind fence we expect a return to updraft conditions (perhaps with a vortex against the fence, having a downdraft along the fence face). During corner flow there is an intense downdraft near the upwind corner of the plot, which probably extends along the upwind portion of the plot diagonal, corresponding to the observed high-speed jet.

The fence also enhances turbulence within the plot, given by the standard deviation of the velocity fluctuations ($\sigma_{u,v,w}$). Vertical turbulence (σ_w) at the plot center is 10%–80% higher than the ambient wind, and during corner flow σ_w in the upwind corner is about double that of the ambient level. Lateral turbulence ($\sigma_u + \sigma_v$) is reduced in the plot, presumably because of the resistance of the fence to lateral fluctuations. Immediately downwind of the plot we expect a quiet zone of reduced turbulence, with a wake zone of enhanced turbulence further downwind (as observed behind a straight fence, e.g., McNaughton 1989).

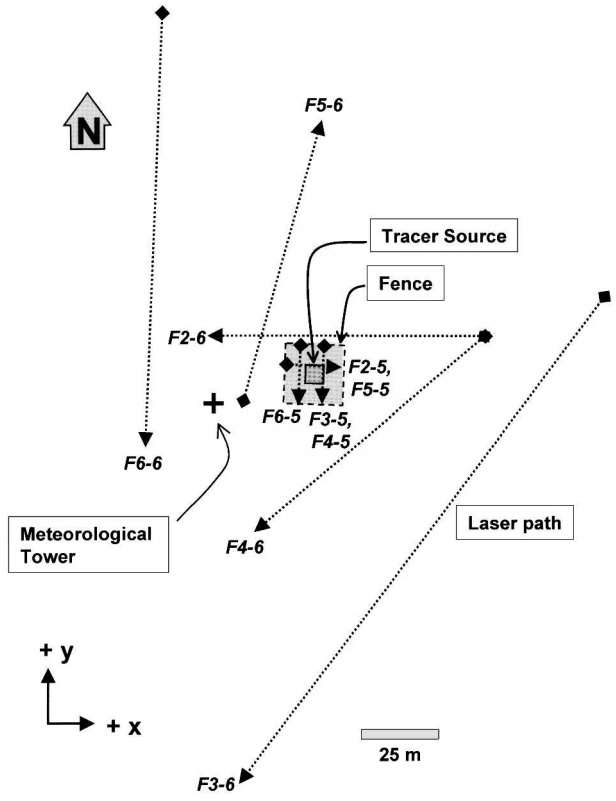

FIG. 3. Map of the laser paths used in the experiment. The trial name associated with each path (e.g., F2–5) is given adjacent to the arrow.

4. Emissions inference

Concentration C_L was measured during $n = 79$ fifteen-minute periods, for path locations that varied from immediately beside the source to approximately 100 m downwind (Fig. 3). For each C_L observation we use the idealized bLS model to calculate $(C_L/Q)_{\text{sim}}$ for the prevailing (u_*, z_0, L, β). But in this disturbed environment where should these wind parameters be measured/inferred? "Ambient" (from the sonic anemometer on an upwind tower) and "in plot" (from the sonic anemometer at the plot center) locations are considered. In our simulations we will assume (falsely) that the parameters calculated at each of these locations in turn defines a horizontally homogeneous MOST surface layer (with the subscript "p" indicating in-plot values).

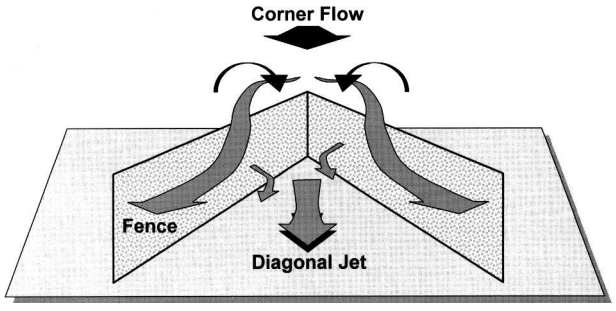

FIG. 4. The conceptual illustration of the flow pattern in the upwind portion of the plot during corner-flow conditions (approach wind oriented along plot diagonal). This is derived from the results in Wilson and Flesch (2003).

Because the in-plot winds differ from the ambient winds, it is no surprise that concurrently calculated wind parameters (u_*, z_0, L, β) at the two locations differ (Fig. 6). And because the relationship between the in-plot and ambient wind varies with the angle of the approaching wind, we see that differences in the two-parameter sets vary with wind angle. For instance, $u_{*\text{p}} \approx u_*$ during corner flow ($\beta_r = 45°$), but $u_{*\text{p}} > u_*$ during normal flow ($\beta_r = 0°$). A similar trend exists for the roughness length z_0. Across all wind angles we find $|L_p| > |L|$ (i.e., our simulations assume a more neutral state when in-plot winds are used). There are also subtle changes in wind direction in the plot. For both normal and corner- flow there does not appear to be any systematic change in direction, but between these extremes there is a deflection $|\beta_p - \beta|$ of 10°–15°.

a. Using ambient winds for Q_{bLS}

In this case we ignore the wind disturbance created by the fence in our bLS simulations, and use (u_*, z_0, L, β) calculated from the upwind anemometer to get Q_{bLS}. Figure 7 shows the Q_{bLS} estimates as a proportion of the actual Q, and plotted versus the downwind distance from the source center to the C_L path (the "fetch"). For any 15-min observation the fetch depends on both the location of the laser path and the prevailing wind direction β. In our experiment the fetch ranges from 3 to 98 m (2.4–78h), with the plot fence lying at an equivalent fetch of 10– 14 m (8–11h), depending on the wind direction.

The average of Q_{bLS}/Q across all $n = 79$ fifteen-minute observations is $\langle Q_{\text{bLS}}/\text{Q}\rangle = 1.10$ (i.e., Q_{bLS} overestimates emissions by an average of 10%), with a standard deviation $\sigma_{Q/Q} = 0.28$. The least accurate estimates are $Q_{\text{bLS}}/Q = 0.51$ and 1.80. We see the following trends when using the ambient wind:

1) On average Q_{bLS} is very accurate when C_L is measured far from the plot. For locations where the laser fetch is greater than 15h—so the concentration observation is further than 5h downwind of the plot fence—the average $\langle Q_{\text{bLS}}/\text{Q}\rangle = 0.99$ ($\sigma_{Q/Q} = 0.20$, $n = 40$). For fetches beyond 45h the $\langle Q_{\text{bLS}}/\text{Q}\rangle = 0.97$. This is a level of accuracy similar to what is expected when the winds are truly undisturbed (i.e., no fence, Flesch et al. 2004).
2) The Q_{bLS} is also accurate for short-fetch cases, in which the plume centerline intersects the laser path inside the plot, but away from any fence (i.e., intersection at least h from the fence). When the fetch is less than 7h the $\langle Q_{\text{bLS}}/\text{Q}\rangle = 0.99$ ($\sigma_{Q/Q} = 0.21$, $n = 21$).

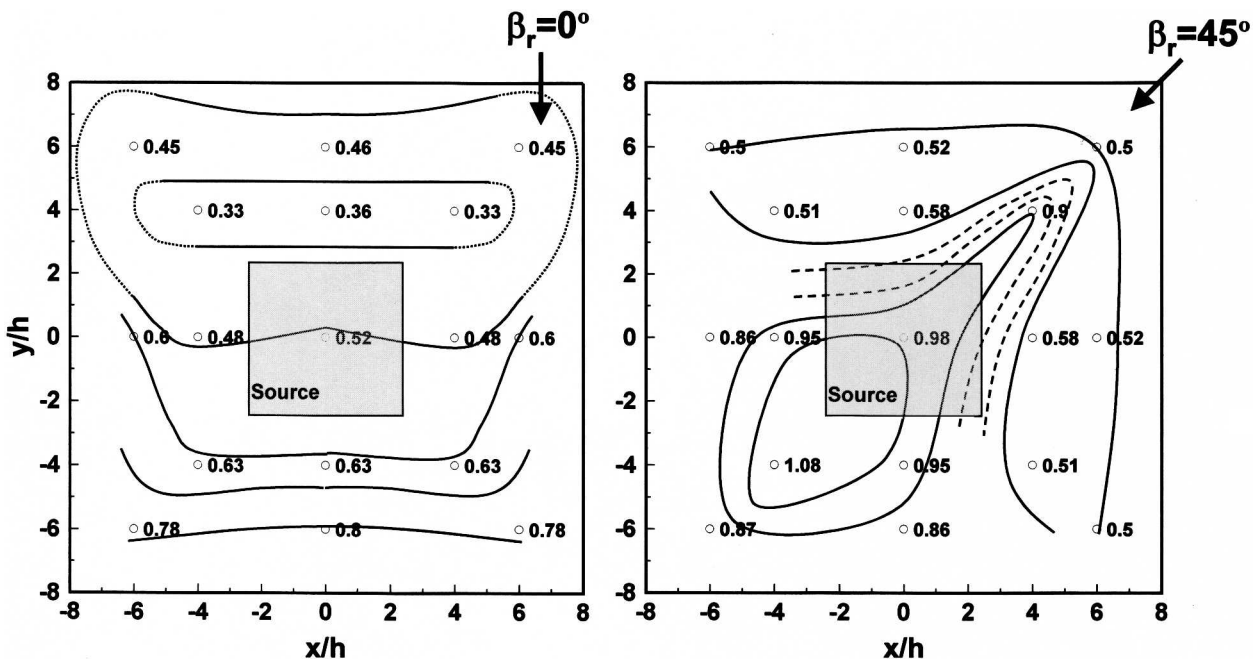

FIG. 5. Hand-drawn contours of the wind speed inside the fenced plot, scaled on the ambient wind speed outside the plot, taken at a height $z/h = 0.5$: (left) normal flow (wind perpendicular to the fence face), and (right) corner flow. The tracer source is given by the shaded square [these data are from Wilson and Flesch (2003)].

3) Systematic overestimation of Q occurs when the laser path is at intermediate fetches, meaning the tracer plume intersects the laser path near a fence. For "near fence" fetches between $7h$ and $15h$ the $\langle Q_{\mathrm{bLS}}/\mathrm{Q}\rangle = 1.47$ ($\sigma_{Q/Q} = 0.19$, $n = 18$).

The good accuracy of Q_{bLS} at the largest fetches is not a surprise. Our hypothesis before the experiment was that at some distance the effect of a local wind disturbance on dispersion is essentially forgotten, that is, is insignificant in defining $(C_L/Q)_{\mathrm{sim}}$. From Fig. 7 we conclude that this threshold distance is somewhere between $5h$ and $35h$ downwind of our plot fence (the limited data within this fetch range does not allow us to specify a more precise location). A similar result can be seen in the modeling study of Tokairin and Kitada (2004), who considered dispersion downwind of a roadbed with and without a surrounding fence.[4] The addition of the fence increased surface concentration approximately 40% near the fence ($2.4h$ from the fence), but by a distance of $10h$ the effect of the fence was less than 5%.

The accuracy of Q_{bLS} in the shortest fetch cases (fetch $< 7h$) was unexpected. In explaining this we note that these cases coincidently correspond to corner-flow (19 of 21 periods have $35° \leq \beta_{\mathrm{r}} \leq 45°$), when u_*, z_0, L, and β are most similar to those calculated from in-plot winds. We conclude that, at least during corner flow, the dispersive environment near the plot center is similar to the ambient wind, and Q_{bLS} inferred from ambient winds are accurate.

The poor accuracy of Q_{bLS} for the near-fence laser positions ($7h <$ fetch $< 15h$) means that in these situations wind complexity cannot be ignored. We imagine two slightly different explanations for the inaccuracy. First, that tracer material is "trapped" by recirculating vortices beside the fence, so that C_L near a fence is higher than predicted with an idealized dispersion model. This would mean it is the near-fence location of C_L that is the problem. Alternatively, the near-fence cases also correspond to normal flow ($\beta_r \leq 25°$), when the in-plot wind parameters are most different from the ambient wind (Fig. 6). Perhaps for normal flow the in-plot winds depart enough from the ambient wind to make for inaccurate Q_{bLS} predictions when C_L is measured inside, or just outside the plot. This suggests that normal-flow conditions explain the errors, and not the near-fence location of C_L. We cannot say which of these two explanations is correct.

b. *Using in-plot winds for Q_{bLS}*

Using $(u_{*p}, z_{0\text{-}p}, L_p, \beta_p)$ provides a simple strategy for incorporating in-plot wind information in the bLS model. This approach has several strengths to recommend it when C_L is measured inside the plot: it will give

[4] Their geometry differed from ours as they simulated a solid fence of infinite crosswind extent on each side of the road, and added a narrow elevated slab above the road (representing an elevated road deck).

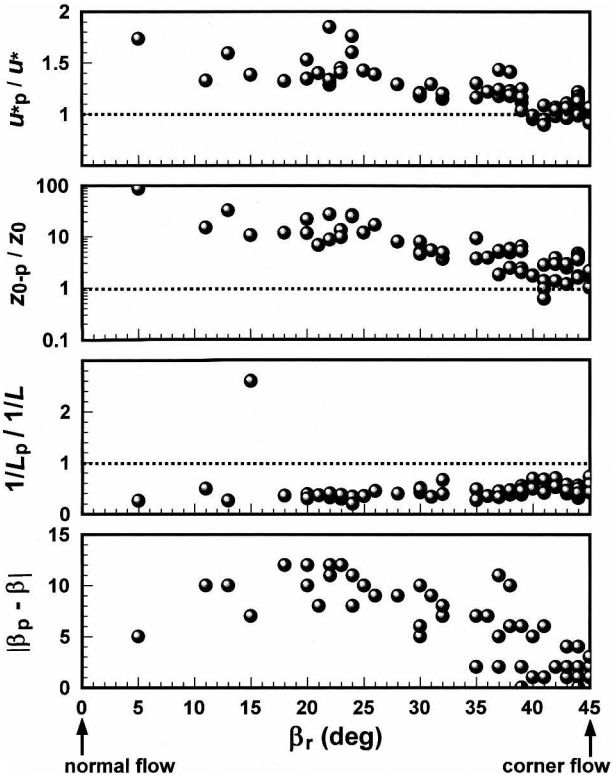

FIG. 6. Relationship of in-plot wind parameters (with subscript "*p*") to the ambient parameters, plotted against the reduced wind angle β_r.

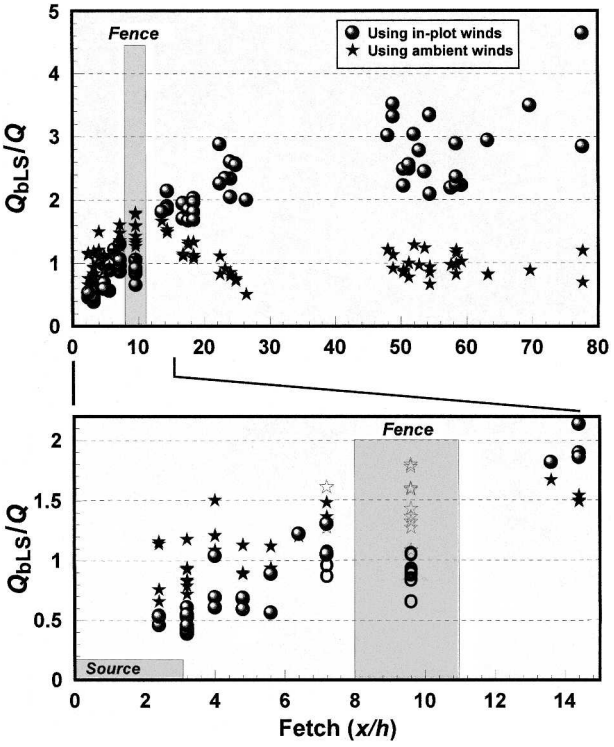

FIG. 7. Ratio of predicted to actual emission rate (Q_{bLS}/Q) plotted vs downwind distance from the source center to the concentration observation C_L (fetch, scaled on fence height h). The Q_{bLS} is calculated using either ambient or in-plot wind parameters. The tracer source and downwind fence positions are indicted by shading (exact locations depend on wind direction). The lower graph expands the short-fetch portion of the top graph. Open symbols on the lower graph indicate normal-flow conditions ($\beta_r \leq 25°$).

an exact fit of the average wind velocity and direction at z_{son} at the plot center; it will give a plausible profile of increasing winds with height away from z_{son}; and it will provide reasonable values for the turbulence (because the turbulent statistics are determined from u_{*p}, which is calculated from actual velocity covariances, this should constrain the turbulence to reasonable values). We assume that using in-plot winds will improve our simulation of dispersion within the plot, and increase the accuracy of Q_{bLS}.

Figure 7 illustrates the Q_{bLS}/Q estimates made using the in-plot wind parameters. Across all laser positions, both inside and outside the plot, the average $\langle Q_{bLS}/Q \rangle = 1.71$ with a standard deviation $\sigma_{Q/Q} = 0.99$ ($n = 79$ observations). This is a lower level of accuracy than found when using ambient wind parameters in the bLS model. We observe the following trends when using in-plot winds:

1) The error in Q_{bLS} increases as C_L is measured further from the plot. For fetches beyond $45h$—meaning further than 35 h downwind of the plot fence—the average $\langle Q_{bLS}/Q \rangle = 2.81$ ($\sigma_{Q/Q} = 0.61$, $n = 23$). The worst individual estimate is $Q_{bLS}/Q = 4.65$, and this occurs at the maximum fetch of $78h$.
2) The Q_{bLS} estimates made using in-plot C_L underpredicts emissions by an average of 25%: $\langle Q_{bLS}/Q \rangle = 0.75$ for fetches less than $10h$ ($\sigma_{Q/Q} = 0.25$, $n = 35$). For these locations we find better accuracy using ambient winds.
3) The Q_{bLS} estimates are most accurate when C_L is measured inside the plot during normal flow. The lower panel of Fig. 7 shows the accuracy of the in-plot locations when $\beta_r \leq 25°$. In these situations $\langle Q_{bLS}/Q \rangle = 0.92$ ($\sigma_{Q/Q} = 0.11$, $n = 12$).

It is no surprise that when concentration is measured far downwind of the plot, using in-plot winds results in large errors in Q_{bLS}. In these cases the in-plot winds do not represent the atmospheric conditions found along most of the path of the dispersing tracer, and using ambient winds in the bLS model is a better choice. But we did not expect this to be true when concentration was measured in the plot, yet this is the case, at least for corner-flow winds.

We explain the limited usefulness of in-plot winds as the result of the large horizontal inhomogeneity of winds in the plot. For example, during corner flow the winds are the most complex, with spatial inhomogeneity of the wind statistics at a maximum (judging from

Wilson and Flesch 2003). In this situation a single in-plot wind observation has limited usefulness in defining the dispersive pattern in the plot. In normal flow the inhomogeneity is reduced over much of the plot (see Fig. 5), which increases the generality of our in-plot observation, and allows some benefit to using in-plot winds when calculating Q_{bLS}.

5. Summary and conclusions

An idealized bLS dispersion model, appropriate for an undisturbed surface layer, was used to infer the emission rate Q_{bLS} from a tracer source placed inside a fenced plot. Despite the wind disturbance caused by the fence, we found surprising accuracy in Q_{bLS} calculated using ambient winds. This accuracy extended to situations where concentration C_L was measured both inside and outside the plot. In the worst cases, where C_L was measured near a fence, Q_{bLS} overestimated Q by an average of 50%. But, if we eliminate these near-fence locations Q_{bLS} averaged within 2% of the true Q (with a standard deviation of about 20%). This is the level of accuracy found when the experiment was performed in a truly undisturbed surface layer (Flesch et al. 2004).

What do these results imply about using idealized inverse-dispersion techniques in nonideal settings? They show that when confronted with a local wind disturbance it is still possible to accurately estimate emissions using a dispersion model that ignores the disturbance. The most appropriate strategy is to take concentration observations well downwind of the disturbance. Once C_L was measured beyond 35 obstacle heights (h) downwind of the plot fence, and possibly beyond only 5h, the effect of the wind perturbation on Q_{bLS}/Q was insignificant (at least for the near-neutral conditions studied here). We speculate that this threshold distance, beyond which the error due to neglecting the disturbance is smaller than the random errors associated with our model predictions, was about 10h from the fence.

Moving 10h (or any specific distance) downwind of an obstacle is unlikely to be a universal threshold for ignoring wind disturbances. The height of the concentration observation z_m will affect this distance. Tokairin and Kitada's (2004) simulations showed that the effect of a fence on downwind concentration was proportionally greater at larger z_m, thus requiring a larger threshold distance (and vice versa for a lower z). We also expect this threshold to relate to features other than h. The rate of wind "recovery" behind an obstacle will be affected by the lateral transport of momentum, and so the extent of shelter will depend on the obstacle width. In our case a wider plot may have required moving further downwind to achieve Q_{bLS} accuracy. The upwind extent of the obstacle will also play a role. Expansive obstacles will perturb the winds over a deeper layer than smaller objects, and increase the distance needed for a return to ambient conditions. The threshold distance may also depend on atmospheric stability (Seginer 1975; Wilson 2004), obstacle geometry (Sakamoto and Arie 1982), and obstacle porosity (McNaughton 1989).

There was no reliable benefit to using in-plot winds when calculating Q_{bLS}. We believe this is due to the large spatial inhomogeneity of the in-plot winds, and the inability of a single wind observation to dependably define the dispersive environment. However, in other settings it may be good strategy to use "within the disturbance" observations when calculating emissions. A feedlot for example, may have sharp horizontal wind gradients concentrated beside widely spaced fences, but may have weak gradients elsewhere. Making concentration and wind observations in the feedlot, but away from fences, may allow for accurate emissions inference. Here it may be better to view the feedlot as having its own interior wind environment, and within that "ambient" environment the fences are the source of the local wind disturbance (a different viewpoint than seeing the feedlot in its entirety as giving a disturbance to the regional ambient winds).

Our results, combined with those of Wilson et al. (2001), suggest that idealized inverse-dispersion techniques can be used in locations with a wind disturbance. In the Wilson et al. study the disturbance was a step change in surface conditions. In this study the wind disturbance was localized, with an eventual return to ambient conditions. In both cases models that assume a homogeneous MOST surface layer were able to infer Q with reasonable accuracy. This indicates that with selectivity in measurement location, inverse-dispersion techniques that assume MOST winds can be accurately applied in disturbed wind conditions.

Acknowledgments. This work has been supported by research grants from the Natural Sciences and Engineering Research Council of Canada (NSERC) and the Canadian Foundation for Climate and Atmospheric Sciences (CFCAS). The useful comments of anonymous reviewers were appreciated.

REFERENCES

Flesch, T. K., J. D. Wilson, L. A. Harper, B. P. Crenna, and R. R. Sharpe, 2004: Deducing ground-to-air emissions from observed trace gas concentrations: A field trial. *J. Appl. Meteor.,* **43,** 487–502.

Garratt, J. R., 1992: *The Atmospheric Boundary Layer.* Cambridge University Press, 316 pp.

Horst, T. W., 1997: A simple formula for attenuation of eddy fluxes measured with first-order response scalar sensors. *Bound.-Layer Meteor.,* **82,** 219–233.

Kaimal, J. C., and J. J. Finnigan, 1994: *Atmospheric Boundary Layer Flows.* Oxford University Press, 289 pp.

Lehning, M., D. R. Shonnard, D. P. Y. Chang, and R. L. Bell, 1994: An inverse algorithm for determining area-source emissions from downwind concentration measurements. *J. Air Waste Manage. Assoc.,* **44,** 1204–1213.

Massman, W. J., 2000: A simple method for estimating frequency response corrections for eddy covariance systems. *Agric. For. Meteor.,* **104,** 185–198.

McInnes, K. J., D. E. Kissel, and E. T. Kanemasu, 1985: Estimating ammonia flux: A comparison between the integrated horizontal flux method and theoretical solutions of the diffusion profile. *Agron. J.,* **77,** 884–889.

McNaughton, K. G., 1989: Micrometeorology of shelter belts and forest edges. *Philos. Trans. Roy. Soc. London,* **B324,** 351–368.

Sakamoto, H., and M. Arie, 1982: Flow around a cubic body immersed in a turbulent boundary layer. *J. Wind Eng. Ind. Aerodyn.,* **9,** 275–293.

Seginer, I., 1975: Atmospheric-stability effect on windbreak shelter and drag. *Bound.-Layer Meteor.,* **8,** 383–400.

Tokairin, T., and T. Kitada, 2004: Numerical investigation of the effect of road structures on ambient air quality—for their better design. *J. Wind Eng. Ind. Aerodyn.,* **92,** 85–116.

Wilson, J. D., 2004: Oblique, stratified winds about a shelter fence. Part I: Measurements. *J. Appl. Meteor.,* **43,** 1149–1167.

——, and T. K. Flesch, 2003: Wind measurements in a square plot enclosed by a shelter fence. *Bound.-Layer Meteor.,* **109,** 191–224.

——, and E. Yee, 2003: Calculation of winds disturbed by an array of fences. *Agric. For. Meteor.,* **115,** 31–50.

——, G. W. Thurtell, G. E. Kidd, and E. G. Beauchamp, 1982: Estimation of the rate of gaseous mass transfer from a surface source plot to the atmosphere. *Atmos. Environ.,* **16,** 1861–1867.

——, T. K. Flesch, and L. A. Harper, 2001: Micrometeorological methods for estimating surface exchange with a disturbed windflow. *Agric. For. Meteor,* **107,** 207–225.